Arch. Metall. Mater. **65** (2020), 2, 917-921

DOI: 10.24425/amm.2020.132839

Y. GARIP[1*]

# PRODUCTION AND MICROSTRUCTURAL CHARACTERIZATION OF Nb-Si BASED IN-SITU COMPOSITE

The Nb-Si based in-situ composite was produced by resistive sintering (RS) technique. In order to identify present phases, X-ray diffraction (XRD) analysis was used on the composite. XRD analysis revealed that the composite was composed of Nb solid solution (Nbss) and α-$Nb_5Si_3$ phases. The microstructure of the composite was characterized by using a scanning electron microscope (SEM). The energy-dispersive spectroscopy (EDS) was performed for the micro-analysis of the chemical species. SEM-EDS analyses show that the microstructure of composite consists of Nbss, $Nb_5Si_3$ and small volume fraction of Ti-rich Nbss phases. The micro hardness of constituent phases of the composite was found to be as 593±19 and 1408±33 $Hv_{0.1}$, respectively and its relative density was % 98.54.

*Keywords:* Nb-Si in-situ composite, Powder Metallurgy, RS, Solid solution strengthening

## 1. Introduction

Niobium silicide based ultrahigh temperature alloys have drawn attention as materials appropriate for the high-temperature applications due to their superior properties such as high melting point, low density, high rigidity and high-temperature strength. [1-3]. The microstructure of the Nb-Si based alloys is typically characterized by the presence of Nb solid solution (Nbss) and niobium silicide ($Nb_5Si_3$, $Nb_3Si$,) [4,5]. The intermetallic compounds (such as $Nb_5Si_3$, $Nb_3Si$ and $Ti_5Si_3$) contribute to oxidation resistance and high-temperature creep while the Nbss enhances the room temperature fracture toughness of the alloy [6,7]. Nbss has superior room temperature fracture toughness exceeding 20 $MPam^{1/2}$ [8] in comparison with $Nb_5Si_3$ phase (2-2.5 $MPam^{1/2}$) [9]. However, their poor oxidation resistance resulting from Nbss and brittleness of niobium silicide are main drawbacks of their practical application [4,6,10].

A great number of studies have been done to get the balance of high temperature strength, ambient temperature fracture toughness and oxidation resistance [4,6]. Alloying and processing technologies are two techniques used for solving these problems [6,11]. Many authors have proposed alloying as the most effective, economical and widely used method to improve the properties of niobium silicide based alloys [10-13]. The influences of Cr [4], Ti [6], Mo [11], B [11], W [11], Al [13], Zn [14], Hf [15] alloying elements on microstructures and mechanical properties of niobium silicide based in-situ composites were reported by many authors. When the Ti addition exceeds 25 at.%, the melting temperature of the Nb-Si alloy reduces bellow 1700°C and $Ti_5Si_3$ phase occurs. It is harmful to the creep resistance of the alloy. [16]. Moreover, alloying these alloys by titanium plays a significant role in improving the fracture toughness by reducing the Peierls-Nabarro barrier energy of Nb [1,17]. Addition of low amounts (less than 5 at. %) of Cr and Al elements contributes to the increase of the high-temperature oxidation resistance [1,10,16]. Mo and W solid solution elements can be used to strengthen the Nb-Si in situ composites. When these elements are used, the composite has been reported to exhibit significantly high compressive strength at temperatures ranging from room temperature to 1500°C [8,18]. Besides, the addition of Mo can contribute to the oxidation resistance improvement of the composite by decreasing oxygen vacancies, which are responsible for oxygen diffuse [19]. Various process techniques such as selective laser melting (SLM) [20,21], hot-pressing sintering [8,22,23], arc melting (AM) [11,17-19,24] and spark plasma sintering (SPS) [17,25,26] are used to prepare the niobium silicide based ultrahigh temperature composites. The resistive sintering (RS) technique has drawn attention as a new powder metallurgy approach for producing intermetallic, ceramics and composites materials. RS process is regarded as an ever-growing

[1] SAKARYA APPLIED SCIENCE UNIVERSITY, TECHNOLOGY FACULTY, DEPARTMENT OF METALLURGY AND MATERIALS ENGINEERING, ESENTEPE CAMPUS, 54187, SAKARYA-TURKE

* Corresponding author: yigitgarip@hotmail.com

and effective fabricating technology [27,28]. The most significant property of RS is that the powder and green compact are heated by the Joule effect and thus, the materials can be synthesized uniformly and rapidly. However, this process is not similar to the rapid solidification method. As a result of this, materials with high density and fine microstructure can be achieved in very short processing time [27-30]. Therefore, RS can be regarded as a potential technique for synthesizing Nb-Si in situ composites. In the literature, it can be seen that the production of these composites by resistive sintering is rare. The aim of this study is producing the at.% Nb-18Si-20Ti-8Al-3Mo-3Cr ultrahigh temperature composite using elemental powders by resistive sintering. There is also much work on Nb-Si or Nb-Si-Ti based alloys. Another aim of this study is to investigate the effects of Al, Mo and Cr alloying elements on the condensation behavior and microstructure of the alloy. The results of the study can provide a reference for the production of Nb-Si-Ti based composites by RS.

## 2. Experimental procedure

A multi-component composite with the nominal composition of (at. %) Nb-18Si-20Ti-5Mo-3Al-3Cr was produced by resistive sintering (RS) technique. The elemental materials used in the current study were Nb (purity 99.8% 40 μm), Ti (purity 99.5%, 40 μm), Si (purity 99.5 %, 1-5 μm), Mo (purity 99.55%, 3-7 μm), Al (purity 99.55%, 7-15 μm) and Cr (99.2%, 10 μm). All elemental powders were provided by Alfa Aesar Company. Prior to the RS, the powders were weighed according to the nominal compositions and then blended in a mechanical mixer for 8 hours to obtain a homogenous powder mixture. The mechanical mixer parameters revealed that the ball-to-powder weight ratio (BPR) was 8:1 and the rotation speed was 210 r/min. The mixed powders of 5 g were inserted into a steel die with an inner diameter of 20 mm. A uniaxial mechanical load of 100 MPa for 1 min. was applied to compact the mixed powders in the die. Afterwards, the compacted powders placed between two counter-sliding punches were synthesized at 4800 amperes and 60 MPa for 35 minutes by RS in air. The electric current applied simultaneously with a uniaxial mechanical load was maintained at the set value throughout RS. After the operation, the sintered specimen inside the die was removed using uniaxial pressure and then air-cooled. Finally, the sintered specimen with dimensions of Ø 20 mm × 5 mm was obtained (Fig. 1).

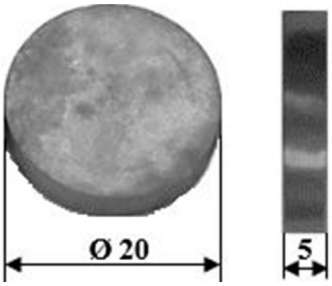


Fig. 1. Digital image of the sintered specimen (unit of measurement is mm)

In order to perform the SEM studies, the sintered specimen was gradually grounded by SiC papers up to 1200 and subsequently polished using 1 μm diamond particles. The specimen was etched by a reagent as follows:

– 7 vol. % $HNO_3$
– 12.5 vol. % HF
– 18.5 vol. % $H_2SO_4$
– 62 vol. % distilled water.

X-ray diffraction analysis (Rigaku, D/MAX-B/2200/PC) was applied to identify the phase constitution of the Nb-Si in-situ composite using diffractometer with Cu Kα radiation and operated at 40 kV and 40 mA. The XRD data scanning angle 2-theta ranges from 20° to 90° with a step size of 0.02°. The microstructure of the composite was observed by a scanning electron microscopy (SEM, JEOL JSM-6060, LV) in a backscattered electron (BSE) mode. Chemical compositions of the constituent present phases were examined by energy-dispersive spectroscopy (EDS, IXRF 5000). In order to obtain standard deviations of the EDS data, five measurements were performed. The relative density of the composite was calculated by Archimedes' principle, based on the immersion technique in distilled water. The micro hardness of constituent phases of the composite was determined by using Vickers diamond indenter. For each phase region, 8 measurements were conducted using the application of a load of 200 g for a dwell time of 10 secs. and measurements were averaged.

## 3. Results and discussion

The morphologies of the powders used as starting material are shown in Fig. 2 (a-f). It can be clearly discerned that the powders of Nb and Ti are sharp-edged while Mo, Al and Cr powders have a spherical shape. However, it was observed that some Mo and Cr particles are agglomerated.

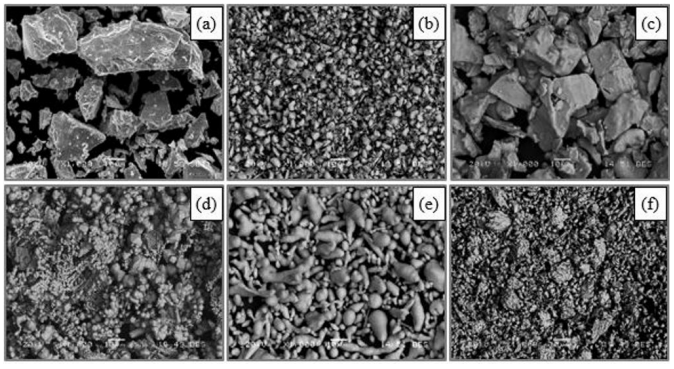


Fig. 2. Morphologies of the elemental powders: (a) Nb, (b) Si, (c) Ti, (d) Mo, (e) Al and (f) Cr

As it can be seen from XRD pattern in Fig. 3, (at.%) Nb-18Si-20Ti-8Al-3Mo-3Cr composite consists of Nb solid solution (bcc, Nbss) and α-$Nb_5Si_3$ ($D8_l$, I4/mcm $Cr_5B_3$ type) phases. The absence of Si and Ti peaks indicates the completed phase transformation. It is worth noting that the niobium solid solution and

$Nb_5Si_3$ phases coexist in a wide range of temperature (from room temperature to 1765°C) and composition (0.5-37.5 Si at.%), as shown in Fig. 4. The $Nb_3Si$ phase decomposed by an eutectoid reaction at approx. 1700°C and leads to the formation of Nbss and $Nb_5Si_3$ phases. According to the Nb-Si binary system, there are two kinds of $Nb_5Si_3$ phases, which are designated as α and β, with tetragonal structures. These phases differ only with respect to their crystal structure type and lattice parameters; α ($Cr_5B_3$-type: at lower temperature (≤1940°C) and β (($W_5Si_3$-type: at higher temperature 1650-2520°C) [16,32]. Furthermore, the lattice parameter of niobium solid solution 0.3288 nm is approx. 0.5% smaller than that of pure niobium (0.3304 nm) [8]. It is considered that the volumetric change of the lattice is affected by the size of the substitution elements.

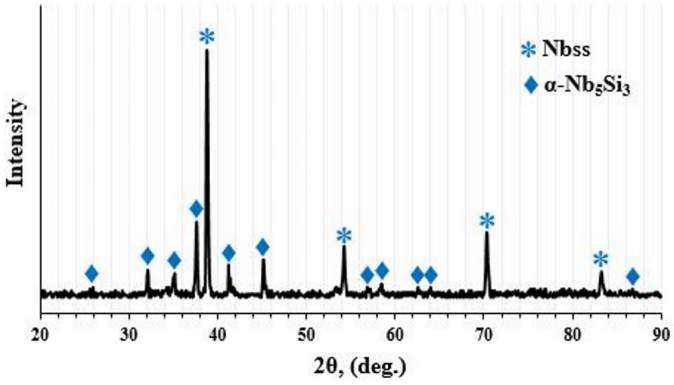


Fig. 3. XRD pattern of (at. %) Nb-18Si-20Ti-8Al-3Mo-3Cr in-situ composite

It should be noted that the RS system has superior properties compared with the conventional sintering process. This process is characterized by the simultaneous application of electric current and mechanical pressure. During RS, the effect of local high temperature provided by Joule effect caused the temperature increase between the particles and resulted in synthesizing the composite. Moreover, this system retarded metastable phases and inhibited grain coarsening or modified in the phase compositions of the formed material due to high heating and cooling rates [29]. Therefore, the original microstructure of the Nb-18Si-20Ti-8Al-3Mo-3Cr composite is maintained, as desired.

When the sintering temperature rises to the melting temperature of Al, liquid phase sintering occurs during the RS process. This increases the density of the composite and reduces the pores. Consequently, the composite with almost full density is obtained by means of electric current and applied pressure.

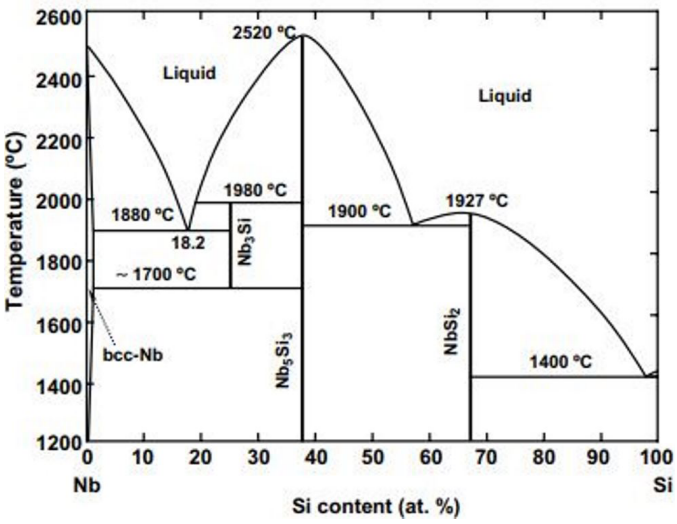


Fig. 4. Nb-Si binary phase diagram [30]

Fig. 5 shows SEM-BSE micrographs of the Nb-18Si-20Ti-8Al-3Mo-3Cr composite. As shown in Fig. 5, the microstructure of the Nb-Si based in-situ composite consists of Nb solid solution, $Nb_5Si_3$ and small volumes of Ti-rich Nbss phases. It can be observed that the regions with gray-white tone are composed of Nbss matrix which is predominant in the microstructure of the composite. Besides, it was distinguished that the $Nb_5Si_3$ with dark-gray tone along with Ti-rich Nbss phases with dark tone distributed in the Nbss matrix. The $Nb_5Si_3$ phase islands are mainly located at the grain boundaries of the Nbss phase. It

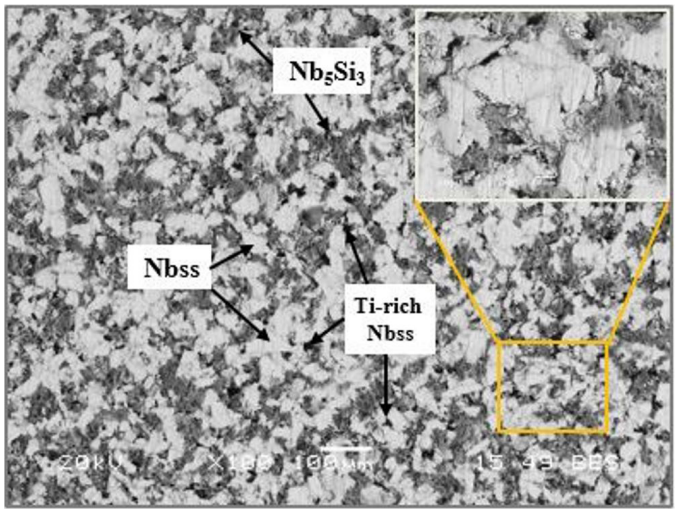


Fig. 5. SEM images of microstructures of Nb-18Si-20Ti-8Al-3Mo-3Cr in-situ composite

TABLE 1

EDS analysis results of the present phases

| Composition | Element (% at.) | | | | | |
|---|---|---|---|---|---|---|
| | Nb | Si | Ti | Al | Mo | Cr |
| Nbss | 56.9±2.48 | 0.7±0.03 | 26.8±1.18 | 9.1±0.57 | 2.4±0.19 | 4.1±0.36 |
| $Nb_5Si_3$ | 45.9±1.87 | 35.2±2.06 | 14.7±1.09 | 2.8±0.21 | 0.6±0.03 | 0.8±0.28 |
| Ti-rich Nbss | 49.5±1.92 | 0.8±0.04 | 37.4±1.35 | 7.2±0.57 | 2.9±0.24 | 2.2±0.18 |

was determined that the Nbss phase was 40 μm in size, while $Nb_5Si_3$ phase had mean dimensions of 10 μm in width and 20 μm in length and most of the Ti-rich Nbss phases had a round shape and mean size of 2 μm.

In respect to the Nb-Si binary phase diagram, the solubility of Si in Nb solid solution is smaller than 0.5 (at.%) at 1600°C, even a minor amount of silicon (atomic radii of 0.115 nm) may significantly decrease the unit cell volume of Nb solid solution [18]. As seen in Table 1, the contents of Si in the Nbss were remarkably smaller than those in the $Nb_5Si_3$. It was reported the Si was mainly present in the silicide phase [19]. Furthermore, the Si content determined the volume fraction of the silicide phase/s and hence played an essential role in the behavior of the creep and fracture toughness of the material [16]. In contrast, the contents of titanium, aluminum, molybdenum and chromium in the Nb solid solution phase were more than those in the $Nb_5Si_3$ phase. Considering the effect of substitutional alloying elements, the atomic radii of pure substances were as follows [33]; Ti (0.146 nm), Mo (0.136 nm) and Al (0.143 nm) were closer to those of Nb (0.143 nm) and thus these elements preferentially substituted for Nb. The reason why Mo was higher in Nbss than in $Nb_5Si_3$ could be attributed to the reasons above. Furthermore, as mentioned before, the lattice parameter of the Nbs could be reduced by substitutional elements.

The bulk density of the composite was calculated using the Eq. (1) [34]:

$$\left(\rho_{bilk}\right)^{-1} = \left( \frac{\text{wt. \%Nb}}{\rho_{\text{Nb}}} + \frac{\text{wt. \%Si}}{\rho_{\text{Si}}} + \frac{\text{wt. \%Ti}}{\rho_{\text{Ti}}} + \frac{\text{wt. \%Al}}{\rho_{\text{Al}}} + \frac{\text{wt. \%Mo}}{\rho_{\text{Mo}}} + \frac{\text{wt. \%Cr}}{\rho_{\text{Cr}}} \right) \quad (1)$$

The density of the composite determined on the basis of Archimedes' was listed in Table 2. The relative density obtained by dividing the experimental density value and the calculated theoretical density value gave information about the porosity amount of the specimen. It could also be noticed from Fig. 5 that the microstructure of the composite had low porosity.

TABLE 2

Density of the Nb-18Si-20Ti-8Al-3Mo-3Cr in-situ composite

| Material | Experimental density (g cm$^{-3}$) | Theoretical density (g cm$^{-3}$) | Relative density (%) |
|---|---|---|---|
| Nb-18Si-20Ti-8Al-3Mo-3Cr | 6.025 | 6.114 | 98.54 |

However, the application of mechanical load, one of the RS parameters, played an important role in the porosity control of RSed materials [28]. It is important to note that the mechanical property of metallic alloys was considerably influenced by their density [34]. The obtained micro hardness values for Nbss and $Nb_5Si_3$ phases in the present study and literature are listed in Table 3.

TABLE 3

The micro hardness values that were measured and obtained from the literature

| Materials | Reference | Nbss | $Nb_5Si_3$ |
|---|---|---|---|
| Nb-18Si-20Ti-8Al-3Mo-3Cr | This study | 593±19 | 1408±33 |
| Nb-20Si-10Mo | [25] | 712±8 | 1760±16 |
| Nb-20Si-10Mo-10W | [25] | 798±10 | 1433±8 |
| Nb–18Si–10Mo–10Ti–15W | [18] | 700 | 1480 |
| Nb-10Si | [35] | 338±41 | — |

It was reported that the Nbs phase (at <1%) demonstrated a hardness of 230-250 Hv with the addition of alloying elements. However, the hardness of this phase could be increased up to 677 Hv depending on the alloying elements [35]. As it can be seen from Table 3, the hardness of the RS alloy was considerably higher than that of the Nbss phase in the binary alloy and was lower than that of the Nb-20Si-10Mo and Nb-20Si-10Mo-10W alloys. This result can be attributed to the fact that the alloying elements Mo, W and Cr significantly increase the micro hardness of these alloys with solid solution strengthening. It was also suggested that the combination of W and Mo alloying elements played a key role in increasing the micro hardness of the Nb solid solution phase [25]. In addition, differences in the hardness values of the alloys can be attributed to the preparation techniques which may narrow the grain sizes, as well as the volume fraction of the silica phases.

## 4. Conclusions

In this study, resistive sintering (RS) technique, which allows the preparation of materials with advanced physical and mechanical properties compared to those obtained with conventional sintering techniques, was used.

The following conclusions can be drawn from this study:

1. Nb-18Si-20Ti-8Al-3Mo-3Cr (at.% ) composite was produced at 4800 A and 60 MPa for 35 minutes by RS in air.
2. XRD analysis revealed that the composite was consisted of a two-phase (Nbss and $Nb_5Si_3$) microstructure, as desired.
3. The micro hardness of constituent phases of the composite was found to be as 593±19 and 1408±33 $Hv_{0.1}$, respectively. The relative density of the composite was % 98.54.

## REFERENCES


[1] B. Kong, L. Jia, L. Su, K. Guan, J. Weng, H. Zhang, Mater. Sci. Eng. A, **639**, 114-121 (2015). doi:10.1016/j.msea.2015.04.096

[2] B. Guo, X. Guo, Mater. Sci. Eng. A, **617**, 39-45 (2014). doi:10.1016/j.msea.2014.08.009

[3] X. Ma, X. Guo, M. Fu, H. Guo, Scripta Mater. **139**, 108-113 (2017). doi:10.1016/j.scriptamat.2017.06.035

[4] Y. Tang, X. Guo, J. Alloy Compd. **731**, 985-994 (2018). doi:10.1016/j.jallcom.2017.10.122

[5] Y. Guo, L. Jia, B. Kong, S. Zhang, J. Sha, H. Zhang, J. Alloy Compd. **696**, 516-521 (2017). doi:10.1016/j.jallcom.2016.11.23

[6] Y. Sainan, J. Lina, S. Linfen, M. Limin, Z. Hu, Intermetallics **38**, 102-106 (2013). doi:10.1016/j.intermet.2013.02.022

[7] W. Kim, H. Tanaka, S. Hanada, Intermetallics **10**, 2002, 625-634 (2002). doi:10.1016/S0966-9795(02)00041-9

[8] J.L. Yu, X.D. Weng, N.L. Zhu, H. Liu, F. Wang, Y.C. Li, X.M. Cai, Z.W. Hu, Intermetallics **90**, 135-139 (2017). doi:10.1016/j.intermet.2017.07.014

[9] P. Tsakiropoulos, Materials **11**, 1-19 (2018). doi:10.3390/ma11010069.

[10] X. Ma, X. Guo, M. Fu, Y. Qiao, Intermetallics **70**, 17-23 (2016). doi:10.1016/j.intermet.2015.11.001

[11] Y. Kang, Y. Yan, J. Song, H. Ding, Mater. Sci. Eng. A, **599**, 87-91 (2014). doi:10.1016/j.msea.2014.01.077

[12] P. Maji, R. Mitra, K.K. Ray, Intermetallics **85**, 34-47 (2017). doi:10.1016/j.intermet.2017.01.012

[13] Y. Guo, L. Jia, B. Kong, H. Zhang, H. Zhang, Intermetallics **92**, 1-6 (2018). doi:10.1016/j.intermet.2017.09.005

[14] M.-L. Wu, S-S. Li, L.-L. Jiang, S.-K. Gong, Y.-F. Han, Pro. Nat. Sci.-Mater. **21**, 139-145 (2011). doi.org/10.1016/S1002-0071(12)60047-1

[15] F. Wang, L. Luo, Y. Xu, X. Meng, L. Wang, B. Han, Y. Su, J. Guo, H. Fu, Intermetallics **88**, 6-13 (2017). doi:10.1016/j.intermet.2017.04.018

[16] K. Zelenitsas, P. Tsakiropoulos, Intermetallics **13**,1079-1095 (2005). doi:10.1016/j.intermet.2005.02.002

[17] T. Fei, Y. Yu, C. Zhou, J. Sha, Mater. Design **116**, 92-98 (2017). doi:10.1016/j.matdes.2016.12.001

[18] J.-H. Kim, T. Tabaru, M. Sakamoto, S. Hanada, Mater. Sci. Eng. A **372**, 137-144 (2004). doi:10.1016/j.msea.2003.12.010

[19] K. Geethasree, Md. Zafir Alam, G. Brahma Raju, V.V. Satya Prasad, Materials Today: Proceedings **15**, 36-43 (2019). doi.org/10.1016/j.matpr.2019.05.021

[20] Y. Guo, L. Jia, B. Kong, F. Zhang, J. Liu, H. Zhang, Corros. Sci. **127**, 260-269 (2017). doi:10.1016/j.corsci.2017.08.022

[21] R. Dicks, F. Wang, X. Wu, J Mater. Process. Tech. **209**, 1754-1757 (2009). doi:10.1016/j.jmatprotec.2008.04.042

[22] J.L. Yu, K.F. Zhang, Scripta Mater. **59**,714-717 (2008). doi:10.1016/j.scriptamat.2008.05.035

[23] J.L. Yu, Z.K. Li, K.F. Zhang, X. Zheng, J.J. Zhang, R. Bai, W.S. Wang, Mater. Sci. Eng. A, **527**, 5230-5233 (2010). doi:10.1016/j.msea.2010.04.068

[24] X. Zhang, Y. Li, X. He, X. Liu, Q. Jiang, Y. Sun, Mater. Sci. Eng. A **646**, 332-340 (2015). doi:10.1016/j.msea.2015.08.014

[25] B. Xiong, C. Cai, Z. Wang, J. Alloy Compd. **583**, 574-577 (2014). doi:10.1016/j.jallcom.2013.08.151

[26] Z. Chen, Y.W. Yan, J. Alloy Compd. **413**, 73-76 (2006). doi:10.1016/j.jallcom.2005.06.005

[27] Y. Garip, O. Ozdemir, J. Alloy Compd. **780**, 364-377 (2019). doi:10.1016/j.jallcom.2018.11.324

[28] S. Grasso, Y. Sakka, G. Maizza, Sci. Technol. Adv. Mater. **10**, 1-24 (2009). doi:10.1088/1468-6996/10/5/053001

[29] Y. Garip, O. Ozdemir, Metall. Mater. Trans. A, **49A**, 2455-2462 (2018). doi:10.1007/s11661-018-4581-8

[30] R. Orru, R. Licheri, A.M. Locci, A. Cincotti, G. Cao, Mater. Sci. Eng. **R 63**, 127-287 (2009). doi:10.1016/j.mser.2008.09.003

[31] Z. Li, L.M. Peng, Acta Mater. **55**, 6573-6585 (2007). doi:10.1016/j.actamat.2007.08.012

[32] J.-C. Zhao, M.R. Jackson, L.A. Peluso, Mater. Sci. Eng. A **372**, 21-27 (2004). doi:10.1016/j.msea.2003.08.008

[33] Y. Zhang, T.T. Zuo, Z. Tang, M.C. Gao, K.A. Dahmen, P.K. Liaw, Z.P. Lu, Prog. Mater. Sci. **61**, 1-93 (2014). doi:10.1016/j.pmatsci.2013.10.001

[34] A.L. Rominiyi, M.B. Shongwe, N. Maledi, B.J. Babalola, P.A. Olubambi, Int. J. Adv. Manuf. Technol. 1041-1049 (2019). doi:10.1007/s00170-019-03950-5

[35] M.G. Mendiratta, J.J. Lewandowski, D.M. Dimiduk, Metall. Mater. Trans. A, **22A**, 1573-1583 (1991). doi:10.1007/BF02667370

[36] S. Kashyap, C.S. Tiwary, K. Chattopadhyay, Mater. Sci. Eng. A **583**, 188-198 (2013). doi:10.1016/j.msea.2013.06.045